Sciencexpress Reports

# Electrically Switchable Chiral Light-Emitting Transistor

**Y. J. Zhang,[1]* T. Oka,[1] R. Suzuki,[1] J. T. Ye,[1,2,3] Y. Iwasa[1,3]***

[1]Quantum-Phase Electronics Center (QPEC) and Department of Applied Physics, University of Tokyo, Tokyo 113-8656, Japan. [2]Zernike Institute for Advanced Materials, University of Groningen, Nijenborgh 4, 9747 AG, Groningen, Netherlands. [3]RIKEN Center for Emergent Matter Science (CEMS), Wako 351-0198, Japan.

*Corresponding author. E-mail: yzhang@mp.t.u-tokyo.ac.jp (Y.J.Z.); iwasa@ap.t.u-tokyo.ac.jp (Y.I.)

**Tungsten diselenide ($WSe_2$) and related transition metal dichalcogenides (TMDs) exhibit interesting optoelectronic properties due to their peculiar band structures originating from the valley degree-of-freedom. While the optical generation and detection of valley polarization has been demonstrated, it has been difficult to realize active valley-dependent functions suitable for device applications. We report an electrically switchable circularly polarized light source based on the material's valley degree-of-freedom. Our $WSe_2$-based ambipolar transistors emit circularly polarized electroluminescence from *p-i-n* junctions electrostatically formed in transistor channels. This phenomenon can be explained qualitatively by the electron–hole overlap controlled by the in-plane electric field. Our device demonstrates a route to exploit the valley degree-of-freedom, and the possibility to develop a valley-optoelectronics technology.**

Circularly polarized light is utilized in various fields ranging from 3D displays to technologies involving effective spin sources in spintronics (*1*) and information carriers in quantum computation (*2*), as well as to induce exotic quantum phenomena such as the Floquet topological state (*3*, *4*). There is a strong demand for circularly polarized light sources having both compactness for achieving a high level of integration and electrical controllability of the polarization. However, currently available light sources are incapable of meeting these requirements; for instance, optical filters (composed of a polarizer and a quarter-wave plate) require mechanical movement to change the polarization, spin light-emitting diodes (LEDs) (*5*) do not work without an external magnetic field, and metamaterials (*6*) or chiral polymer LEDs (*7*) can produce only a fixed circular polarization with a specific material configuration. Circularly polarized luminescence from solids is known to be a consequence of direct-gap interband transitions of electrons from the conduction band to the valence band with a total angular momentum shift of ±1. Thus, in order to achieve electrical controllability of the polarization of the luminescence, the minimum requirement is that these transitions must be associated with a degree-of-freedom that responds to an electric field.

Transition-metal dichalcogenides (TMDs), especially in the monolayer limit, is a promising candidate for such devices since two interband transitions are associated with not only the spin degree-of-freedom but also the momentum degree-of-freedom (*8*), which is indeed related to the electrical current. Monolayers of TMDs consist of a triangularly aligned transition-metal (typically Mo or W) plane sandwiched by two triangularly aligned chalcogen (typically S or Se) planes. Each metal atom is surrounded by six chalcogen atoms, forming a trigonal prismatic structure (Fig. 1A). Monolayer TMD shares many properties with graphene-like materials with different A- and B-site atoms in which inversion symmetry is broken (*9*). In monolayer TMD, electron and hole valleys exist at K and K' points in the hexagonal Brillouin Zone, leading to a direct-gap semiconductor nature (Fig. 1B). Because the electronic states of the two valleys have different chiralities due to the inversion asymmetric crystal structure, interband transitions at K and K' points are allowed for $\sigma_+$ and $\sigma_-$ circularly polarized light, respectively (valley circular dichroism) (*8*). These features are suppressed in bulk single crystals because the inversion symmetry is recovered whilethe band structure change from direct gap to indirect gap (*10*).

Circularly polarized photoluminescence (PL) from TMDs has been experimentally observed for monolayers (*11*–*15*) and for biased bilayers (*16*) when they were pumped with circularly polarized incident light. Here, we report current-induced circularly polarized electroluminescence (EL) from *p-i-n* junctions in monolayer and multilayer tungsten diselenide ($WSe_2$) (*17*). Moreover, the polarization was found to be electrically controllable by changing the current direction.

*P-i-n* junctions were formed using an electric-double-layer transistor (EDLT) structure with $WSe_2$ thin flakes having thicknesses of 0.6–2.6 nm as the channel material (*18*). Since TMD-FETs show ambipolar transistor behavior (*19*–*24*), controlling the potential difference between the gate, source, and drain electrodes enables simultaneous accumulation of both electrons and holes inside the channel (Fig. 1C), leading to light emission from the *p-i-n* junction, as demonstrated in organic ambipolar FETs (*25*, *26*). EDLT-induced carriers in the channels can be electrostatically fixed when the device is cooled down under such bias conditions, forming a bias-independent *p-i-n* junction (Fig. 1D) (*19*).

EDLT has an additional benefit of eliminating the strong limitation of monolayers (*27*–*30*). Naively thinking, multilayers (bulk material) are not suited for realizing circularly polarized EL. The restored inversion symmetry suppresses valley circular dichroism. In addition, multilayers are indirect-gap semiconductors, where the conduction band minimum and the valence band maximum locate at T and Γ points, respectively (*10*). EDLTs can overcome these difficulties. First, the gate electric field breaks the inversion symmetry (*16*, *24*). This recovers the peculiar features of monolayers, including valley circular dichroism (*16*). Second, because EDLTs produce an electric field one order of magnitude stronger than conventional FETs do, drastic band modulations occur: the valence band top is replaced by K points, and the energy difference between T and K points of the conduction band gets smaller (*24*). By combining these band structure changes with the large carrier accumulation capability of EDLTs (~$1 \times 10^{14}$ $cm^{-2}$), not only holes but also electrons can populate the K points. Therefore, multilayers under an ELDT operates in a similar manner as monolayers (*24*).

Typical transistor characteristics of our $WSe_2$ EDLTs are displayed in Fig. 1E (transfer curve) and Fig. 1F (output curve), showing clear ambipolar operation. The carrier density and carrier mobility are estimated to be of the order of $10^{13}$ $cm^{-2}$ and $10^2$ $cm^2/Vs$, respectively. As demonstrated in Ref. 19, we controlled $V_G$ and $V_{DS}$ to drive our transistor into the ambipolar region in the output curve measurement (Fig. 1G, red curve) and cooled it down to 160 K to freeze the gate dielectric, forming a bias independent *p-i-n* junction. $I_{DS}$ showed a contrasting response at 160 K, with a clear rectifying operation (Fig. 1G, blue curve). The rectification was further confirmed by a log-scale plot shown in Fig. 1H.

When the $WSe_2$ *p-i-n* junction was forward biased, clear EL was observed, as shown in Fig. 2A. To enhance the EL efficiency, all spectra were recorded at 100 K unless otherwise specified. Two features should

be emphasized. First, all EL spectra showed net circular polarization. The degree of circular polarization, defined as $\eta = (I(\sigma_+) - I(\sigma_-)) / (I(\sigma_+) + I(\sigma_-))$, reached as high as 45% (device #1 at 40 K), which is comparable to that of PL from monolayers (*12*–*14*). Second, such circularly polarized EL was clearly observed even in multilayer samples (devices #2, #3, and #5), as explained above (*18*). The EL intensity increased with increasing bias voltage (Fig. 2B). The total intensity depended linearly on the forward current (Fig. 2C), whereas η and the external quantum efficiency (EQE) showed smaller current dependence (Figs. 2, D and E). The EQE value depended on the samples and ranged from $2\times10^{-5}$ to $6\times10^{-4}$, which is larger than that of the emissions from contact Schottky diodes (*27*), possibly due to the location of the emission zone in our devices, which is away from the contacts.

Figure 2A indicates that the EL spectral shape depended on the samples, and all of them can be considered as a superposition of exciton emission around 1.66 eV (by comparing with the PL spectrum in Fig. 2F) and trion emission at lower energies, which have been observed in PL from electrostatically charged TMDs (*14*, *15*, *31*). The variation of the trion emission energy can be ascribed to the difference in doping concentrations among the samples (*14*). The emission type is expected to be controlled by carrier injection into the *i*-region (*18*).

Figure 3A shows the EL spectra of a single device for two opposite current directions. Because the ionic liquid freezes at 100 K, the source and drain biases were exchanged after the device was warmed up to 220 K, followed by another cooling before the next EL measurement (*32*). Importantly, the circular polarization was reversed when the source–drain bias was exchanged. This is the first demonstration of electrical control of circularly polarized luminescence. The EL spectral shape was also changed from an exciton-dominant one to a trion-dominant one, possibly due to the difference in doping profiles between the two bias directions (*18*).

According to the band structure of monolayer TMDs (Fig. 1B), circularly polarized luminescence only occurs when K and K' valleys make inequivalent contributions. Here, we suggest a possible model from the viewpoint of semi-classical transport theory (*33*), which gives information of the carrier distribution under an electric field. Under a static electric field, the hole distribution shifts parallel to the field in the momentum space, whereas the electron distribution shifts to the opposite direction. As a result, the electron–hole overlap shown in Fig. 3B differ between the two valleys (valley overlap polarization, VOP) because the carrier distributions in TMDs are not isotropic due to trigonal warping (*34*). VOP provides an intensity difference in the luminescence from two valleys, leading to circularly polarized luminescence. The above scenario is widely applicable to TMDs which have two isolated anisotropic valleys with different chiralities. In addition to the observations in $WSe_2$, circularly polarized EL has also been observed in $MoSe_2$ and $MoS_2$ (*18*).

A numerical calculation was performed based on this model (*18*). To understand the carrier distribution in the momentum space, we combined the Boltzmann equation (*33*) and the charge distribution equation for a *p*-*n* junction (*35*) (for simplicity, a *p*-*n* junction model was used rather than a *p*-*i*-*n* junction). The effects of excitons and trions were ignored since we are only interested in the asymmetry. As shown in Fig. 4A, the band dispersions, especially that of the valence band, is anisotropic due to trigonal warping (*34*). When an in-plane electric field is applied, the charge distribution is shifted from its equilibrium position (Fig. 4B). Importantly, the consequent electron–hole overlap differs between K and K' points giving rise to VOP. Simulated luminescence spectra from K and K' points, corresponding to $\sigma_+$ and $\sigma_-$, respectively, are shown in Fig. 4C. The obtained polarization is qualitatively consistent with the experimental results.

Since trigonal warping is related to the crystal symmetry ($\hat{C}_3$), this scenario indicates that η and the luminescence intensity are quite sensitive to the relative angle between the crystal orientation and the field direction, exhibiting three-fold symmetry with respect to the rotation of the electric field direction, as clearly shown in the simulated results in Fig. 4D. Hence, if the current path is not perpendicular to the contact, η do not completely reverse its sign when the electrodes are exchanged as shown in Fig. S6. On the other hand, this feature will enable fine tuning of η by using a multi-terminal device to apply biases in directions that are non-parallel to the *p*-*i*-*n* junction (Fig. S7). To maximize the luminescence intensity, the degree of polarization (value of *η)*, and the polarization tunability (tunability of η), it will be necessary to improve the device fabrication processes to accurately align the crystal orientation and electrode configuration.

Circularly polarized EL is a direct indication of the breakdown of valley symmetry. In our experiment, this was induced purely by the electric field, and we had to go beyond linear response theory to understand this phenomenon; for example, we were not able to explain this by the valley Hall effect (*8*). Therefore, we proposed a model that incorporates non-linear processes from the carrier distribution shift which becomes asymmetric due to trigonal warping, leading to VOP.

Owing to their spin-valley coupled band structure (*8*), TMD-based spin LEDs can also exhibit circularly polarized EL. However, such devices cannot work without an external magnetic field (*1*). Our results, on the other hand, provide a new direction in the quest for electrically switchable circularly polarized light sources, and extend the functionality of valley-based optoelectronics.

**References and Notes**


1. I. Žutić, J. Fabian, S. Das Sarma, Spintronics: Fundamentals and applications. *Rev. Mod. Phys.* **76**, 323–410 (2004). doi:10.1103/RevModPhys.76.323
2. J. F. Sherson, H. Krauter, R. K. Olsson, B. Julsgaard, K. Hammerer, I. Cirac, E. S. Polzik, Quantum teleportation between light and matter. *Nature* **443**, 557–560 (2006). doi:10.1038/nature05136 Medline
3. T. Oka, H. Aoki, *Phys. Rev. B* **79**, 081406(R) (2009).
4. Y. H. Wang, H. Steinberg, P. Jarillo-Herrero, N. Gedik, Observation of Floquet-Bloch states on the surface of a topological insulator. *Science* **342**, 453–457 (2013). doi:10.1126/science.1239834 Medline
5. R. Fiederling, M. Keim, G. Reuscher, W. Ossau, G. Schmidt, A. Waag, L. W. Molenkamp, *Nature* **402**, 787–790 (1999). doi:10.1038/45502
6. K. Konishi, M. Nomura, N. Kumagai, S. Iwamoto, Y. Arakawa, M. Kuwata-Gonokami, Circularly polarized light emission from semiconductor planar chiral nanostructures. *Phys. Rev. Lett.* **106**, 057402 (2011). doi:10.1103/PhysRevLett.106.057402 Medline
7. Y. Yang, R. C. da Costa, D. M. Smilgies, A. J. Campbell, M. J. Fuchter, Induction of circularly polarized electroluminescence from an achiral light-emitting polymer via a chiral small-molecule dopant. *Adv. Mater.* **25**, 2624–2628 (2013). doi:10.1002/adma.201204961 Medline
8. D. Xiao, G. B. Liu, W. Feng, X. Xu, W. Yao, Coupled spin and valley physics in monolayers of MoS2 and other group-VI dichalcogenides. *Phys. Rev. Lett.* **108**, 196802 (2012). doi:10.1103/PhysRevLett.108.196802 Medline
9. Z. Y. Zhu, Y. C. Cheng, U. Schwingenschlögl, *Phys. Rev. B* **84**, 153402 (2011). doi:10.1103/PhysRevB.84.153402
10. A. Splendiani, L. Sun, Y. Zhang, T. Li, J. Kim, C. Y. Chim, G. Galli, F. Wang, Emerging photoluminescence in monolayer MoS2. *Nano Lett.* **10**, 1271–1275 (2010). doi:10.1021/nl903868w Medline
11. K. F. Mak, K. He, J. Shan, T. F. Heinz, Control of valley polarization in monolayer MoS2 by optical helicity. *Nat. Nanotechnol.* **7**, 494–498 (2012). doi:10.1038/nnano.2012.96 Medline
12. H. Zeng, J. Dai, W. Yao, D. Xiao, X. Cui, Valley polarization in MoS2 monolayers by optical pumping. *Nat. Nanotechnol.* **7**, 490–493 (2012). doi:10.1038/nnano.2012.95 Medline
13. T. Cao, G. Wang, W. Han, H. Ye, C. Zhu, J. Shi, Q. Niu, P. Tan, E. Wang, B. Liu, J. Feng, Valley-selective circular dichroism of monolayer molybdenum disulphide. *Nat. Commun.* **3**, 887 (2012). doi:10.1038/ncomms1882 Medline

14. A. M. Jones, H. Yu, N. J. Ghimire, S. Wu, G. Aivazian, J. S. Ross, B. Zhao, J. Yan, D. G. Mandrus, D. Xiao, W. Yao, X. Xu, Optical generation of excitonic valley coherence in monolayer WSe2. *Nat. Nanotechnol.* **8**, 634–638 (2013). doi:10.1038/nnano.2013.151 Medline
15. K. F. Mak, K. He, C. Lee, G. H. Lee, J. Hone, T. F. Heinz, J. Shan, Tightly bound trions in monolayer MoS2. *Nat. Mater.* **12**, 207–211 (2013). doi:10.1038/nmat3505 Medline
16. S. Wu, J. S. Ross, G.-B. Liu, G. Aivazian, A. Jones, Z. Fei, W. Zhu, D. Xiao, W. Yao, D. Cobden, X. Xu, Electrical tuning of valley magnetic moment through symmetry control in bilayer MoS2. *Nat. Phys.* **9**, 149–153 (2013). doi:10.1038/nphys2524
17. Y. Song, H. Dery, Transport theory of monolayer transition-metal dichalcogenides through symmetry. *Phys. Rev. Lett.* **111**, 026601 (2013). doi:10.1103/PhysRevLett.111.026601 Medline
18. Materials and methods are available as supplementary materials on *Science* Online.
19. Y. J. Zhang, J. T. Ye, Y. Yomogida, T. Takenobu, Y. Iwasa, Formation of a stable p-n junction in a liquid-gated MoS2 ambipolar transistor. *Nano Lett.* **13**, 3023–3028 (2013). doi:10.1021/nl400902v Medline
20. V. Podzorov, M. E. Gershenson, Ch. Kloc, R. Zeis, F. Bucher, High-mobility field-effect transistors based on transition metal dichalcogenides. *Appl. Phys. Lett.* **84**, 3301–3303 (2004). doi:10.1063/1.1723695
21. Y. Zhang, J. Ye, Y. Matsuhashi, Y. Iwasa, Ambipolar MoS2 thin flake transistors. *Nano Lett.* **12**, 1136–1140 (2012). doi:10.1021/nl2021575 Medline
22. J. T. Ye, Y. J. Zhang, R. Akashi, M. S. Bahramy, R. Arita, Y. Iwasa, Superconducting dome in a gate-tuned band insulator. *Science* **338**, 1193–1196 (2012). doi:10.1126/science.1228006 Medline
23. D. Braga, I. Gutiérrez Lezama, H. Berger, A. F. Morpurgo, Quantitative determination of the band gap of WS2 with ambipolar ionic liquid-gated transistors. *Nano Lett.* **12**, 5218–5223 (2012). doi:10.1021/nl302389d Medline
24. H. T. Yuan, M. S. Bahramy, K. Morimoto, S. Wu, K. Nomura, B.-J. Yang, H. Shimotani, R. Suzuki, M. Toh, C. Kloc, X. Xu, R. Arita, N. Nagaosa, Y. Iwasa, Zeeman-type spin splitting controlled by an electric field. *Nat. Phys.* **9**, 563–569 (2013). doi:10.1038/nphys2691
25. J. Zaumseil, R. H. Friend, H. Sirringhaus, Spatial control of the recombination zone in an ambipolar light-emitting organic transistor. *Nat. Mater.* **5**, 69–74 (2006). doi:10.1038/nmat1537
26. S. Z. Bisri, T. Takenobu, K. Sawabe, S. Tsuda, Y. Yomogida, T. Yamao, S. Hotta, C. Adachi, Y. Iwasa, p-i-n Homojunction in organic light-emitting transistors. *Adv. Mater.* **23**, 2753–2758 (2011). doi:10.1002/adma.201004572 Medline
27. R. S. Sundaram, M. Engel, A. Lombardo, R. Krupke, A. C. Ferrari, P. Avouris, M. Steiner, Electroluminescence in single layer MoS2. *Nano Lett.* **13**, 1416–1421 (2013). Medline
28. A. Pospischil, M. M. Furchi, T. Mueller, *Nat. Nanotech.* doi: 10.1038/nnano.2014.14 (2014).
29. B. W. H. Baugher, H. O. H. Churchill, Y. Yang, P. Jarillo-Herrero, *Nat. Nanotech.* doi: 10.1038/nnano.2014.25 (2014).
30. J. Ross *et al*., *Nat. Nanotech.* doi: 10.1038/nnano.2014.26 (2014).
31. J. S. Ross, S. Wu, H. Yu, N. J. Ghimire, A. M. Jones, G. Aivazian, J. Yan, D. G. Mandrus, D. Xiao, W. Yao, X. Xu, Electrical control of neutral and charged excitons in a monolayer semiconductor. *Nat. Commun.* **4**, 1474 (2013). doi:10.1038/ncomms2498 Medline
32. This process is not essential for circularly polarized EL and polarization reversal. Also, electrical switching can be achieved with solid gate devices in principle.
33. N. W. Ashcroft, N. D. Mermin, *Solid State Physics* (Thomson Learning, US, 1976), chap. 12.
34. A. Kormányos, V. Zólyomi, N. D. Drummond, P. Rakyta, G. Burkard, V. I. Fal'ko, Monolayer MoS_2: Trigonal warping, the Γ valley, and spin-orbit coupling effects. *Phys. Rev. B* **88**, 045416 (2013). doi:10.1103/PhysRevB.88.045416
35. S. M. Sze, *Physics of Semiconductor Devices* (Wiley, New York, 1981), chap. 1, 2.
36. G. Prasad, N. N. Rao, O. N. Srivastava, Growth, structural characteristics and photoelectrochemical behaviour of tungsten diselenide (WSe2) single crystals. *Cryst. Res. Technol.* **21**, 1303–1311 (1986). doi:10.1002/crat.2170211012
37. G. K. Solanki, D. N. Gujaranthi, M. P. Deshpande, D. Lakshminarayana, M. K. Agarwal, Transport property measurements in tungsten sulphoselenide single crystals grown by CVT technique. *Cryst. Res. Technol.* **43**, 179–185 (2008). doi:10.1002/crat.200711060
38. A. K. Geim, K. S. Novoselov, The rise of graphene. *Nat. Mater.* **6**, 183–191 (2007). doi:10.1038/nmat1849 Medline
39. T. Korn, S. Heydrich, M. Hirmer, J. Schmutzler, C. Schüller, Low-temperature photocarrier dynamics in monolayer MoS2. *Appl. Phys. Lett.* **99**, 102109 (2011). doi:10.1063/1.3636402
40. A. Ramasubramaniam, Large excitonic effects in monolayers of molybdenum and tungsten dichalcogenides. *Phys. Rev. B* **86**, 115409 (2012). doi:10.1103/PhysRevB.86.115409

**Acknowledgments:** We thank Y. Saito, H. Shioya, Y. Kasahara, T. Hatano, and Y. Segawa for experimental help and R. Akashi, R, Arita, T. Takenobu, H. Aoki, and B. P. Zhang for discussions. Y.J.Z. is supported by the Japan Society for the Promotion of Science (JSPS) through a research fellowship for young scientists. This research was supported by the Strategic International Collaborative Research Program (SICORP-LEMSUPAR) of the Japan Science and Technology Agency, Grant-in-Aid for Specially Promoted Research (No. 25000003), and the "Funding Program for World-Leading Innovative R&D on Science and Technology (FIRST Program)" from JSPS.

**Supplementary Materials**

www.sciencemag.org/content/science.1251329/DC1
Materials and Methods
Supplementary text
Fig. S1 to S7
References (*36–40*)

27 January 2014; accepted 4 April 2014
Published online 17 April 2014
10.1126/science.1251329

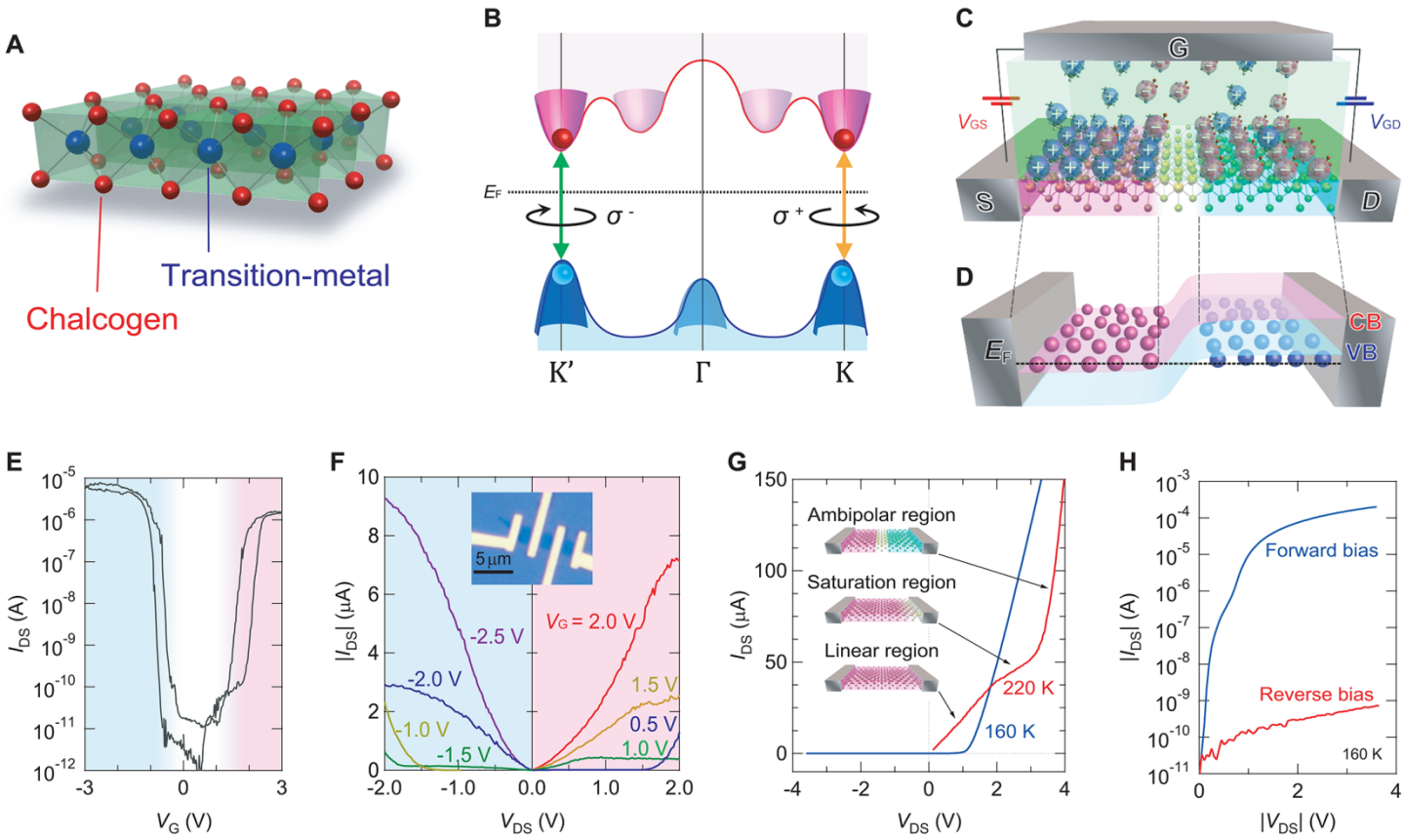


**Fig. 1. Electric double layer transistors in action.** (**A**) Crystal structure of monolayer TMD. (**B**) Illustration of the band structure of monolayer TMD. (**C**) Device structure of TMD EDLT under ambipolar charge accumulation. (**D**) Schematic band structure of EDLT-induced *p-i-n* junction under equilibrium. (**E**) Transfer curve ($I_{DS}$ vs. $V_G$) of monolayer $WSe_2$ EDLT. (**F**) Output curve ($I_{DS}$ vs. $V_{DS}$) of $WSe_2$ EDLT. (Inset) Typical optical micrograph of the device. (**G**) *I–V* characteristics of $WSe_2$ EDLT at 220 K and 160 K, which are higher and lower than the glass transition temperature of DEME-TFSI, respectively. Illustrations show charging status at 220 K. (**H**) Log $|I_{DS}|$ vs. $|V_{DS}|$ plot of the blue curve in G.

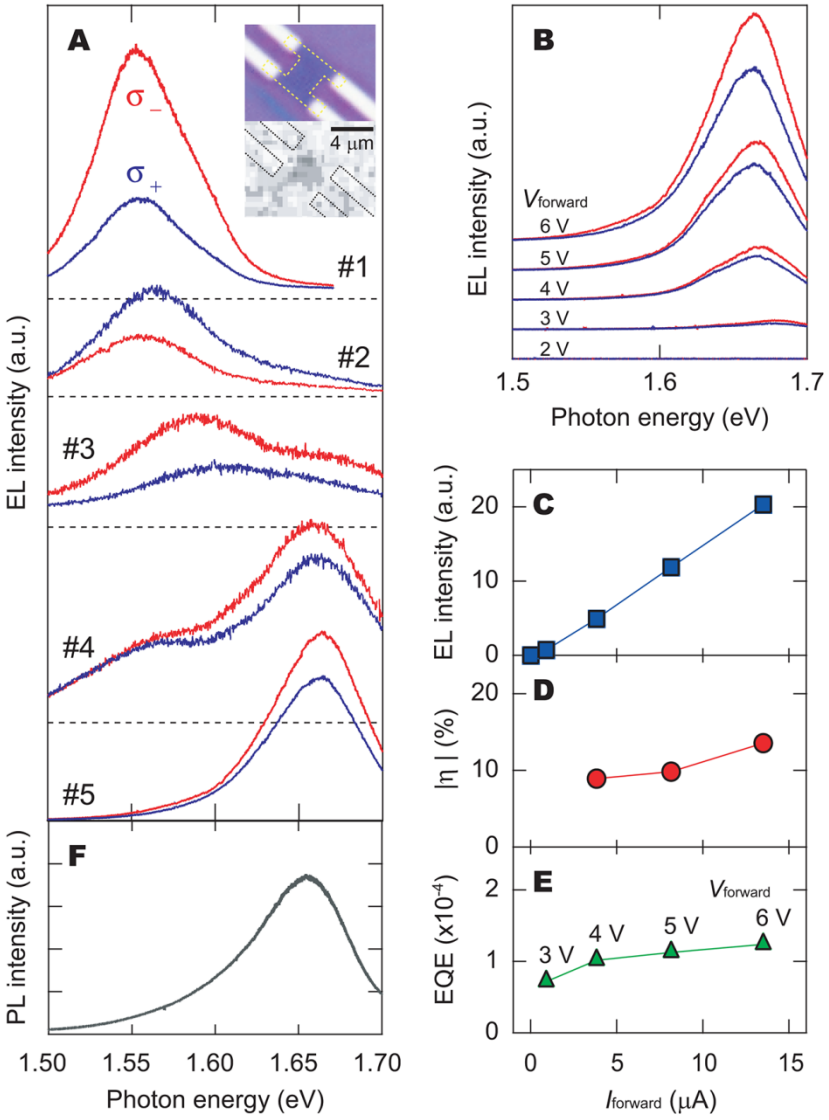


**Fig. 2. Circularly polarized electroluminescence.** (**A**) Polarized EL spectra from five devices. Spectra of device #1 were measured at 40 K. (Inset) Optical micrograph of device #2 and CCD image of EL. The yellow dotted curves denote $WSe_2$ thin flakes. (**B**) Voltage dependence of EL spectra of device #5. (**C**) Current dependence of total EL intensity extracted from Fig. 2B. (**D**) Current dependence of EL polarization extracted from Fig. 2B. (**E**) Current dependence of external quantum efficiency extracted from Fig. 2B. (**F**) PL spectrum of monolayer $WSe_2$ pumped by a He-Ne laser (1.97 eV).

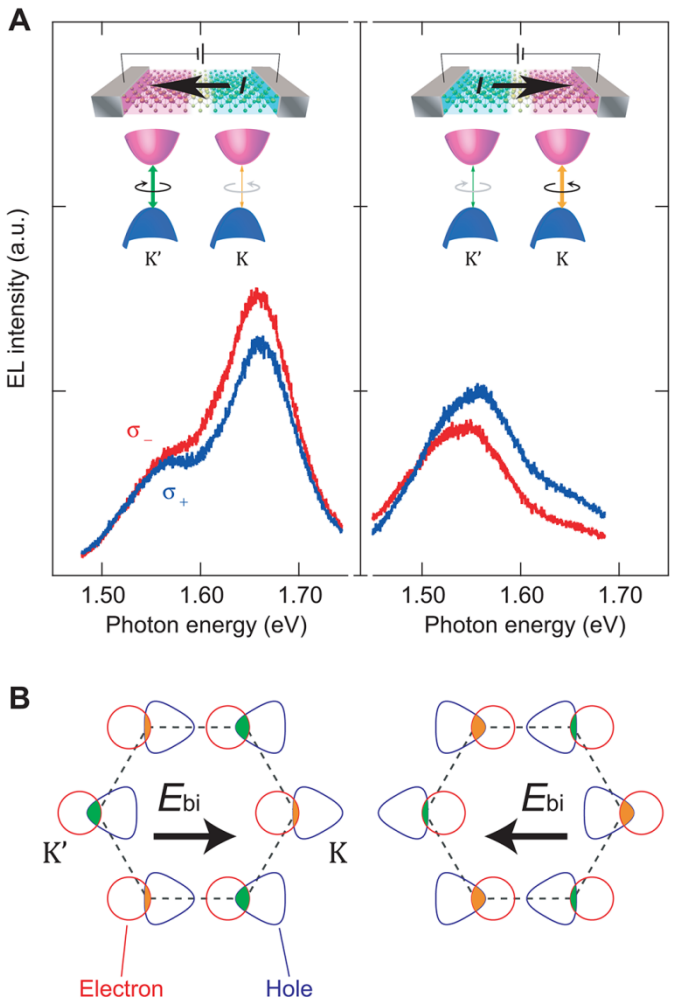


**Fig. 3. Electrical control of circularly polarized emission.** (**A**) Circularly polarized EL spectra from device #4 for two opposite current directions schematically indicated in the upper illustration. Lower illustrations represent the contribution to EL from two valleys. (**B**) Schematic illustrations of electron and hole distributions shifted by the electric fields originating from the built-in potential. Red and blue lines represent contours of electron and hole distributions, respectively. Orange and green areas represent the electron–hole overlap for K and K' valleys, respectively.

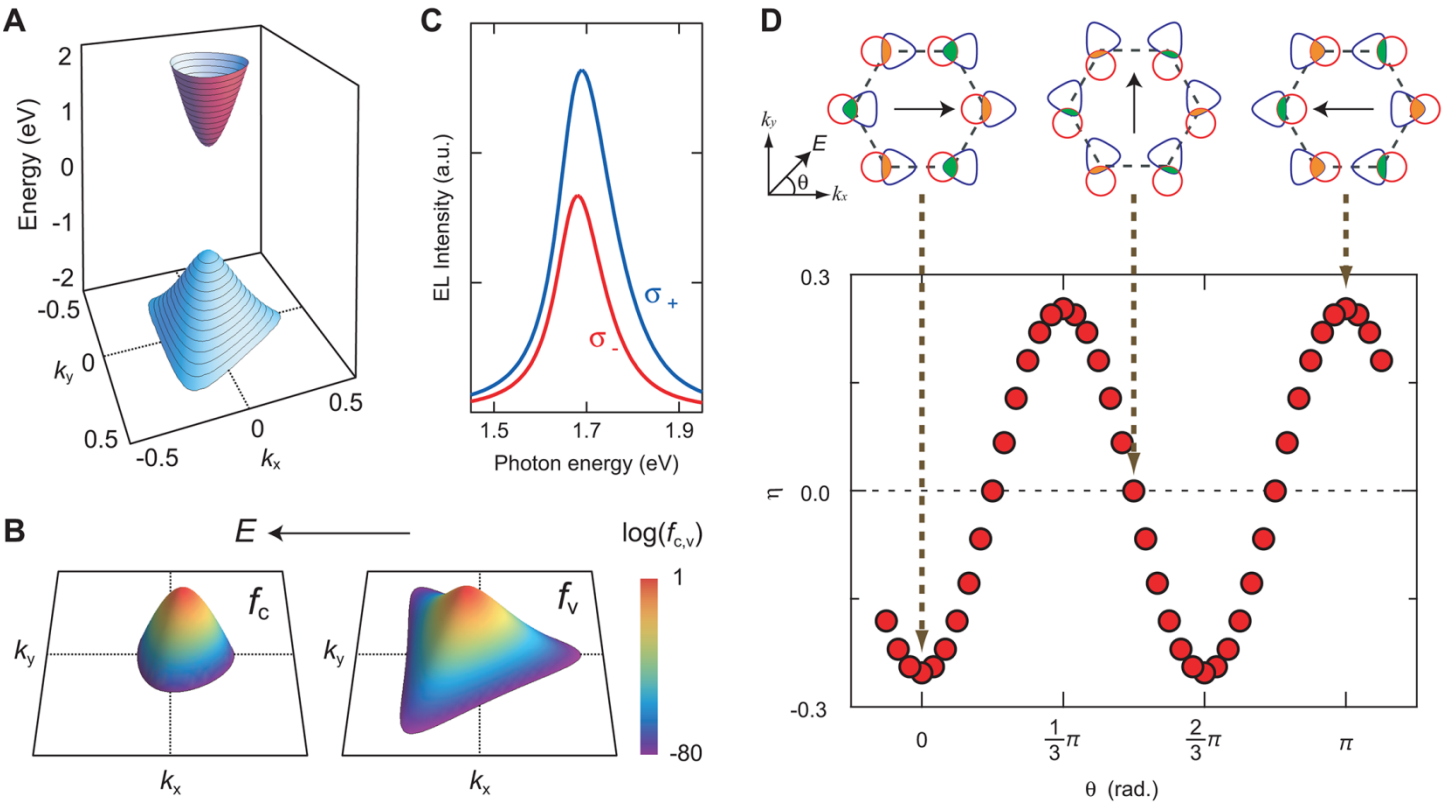


**Fig. 4. Simulation of circularly polarized electroluminescence.** (**A**) Schematic band structure around K point. $k_x$ and $k_y$ are measured from K point. (**B**) Color plot of charge distribution for electron at conduction band ($f_c$) and hole at valence band ($f_v$) around K point. Dotted lines denote $k_x = 0$ and $k_y = 0$. (**C**) Simulated EL spectra from K point ($\sigma_+$) and K' point ($\sigma_-$). (**D**) η vs. electric field direction. The angle θ is measured from the $k_x$ direction. VOPs are shown in top illustrations for three electric field directions along Γ-K (θ = 0°), Γ-M (90°), and Γ-K' (180°).